ARTICLE IN PRESS

Available online at www.sciencedirect.com

ScienceDirect

Ceramics International ▮ (▮▮▮▮) ▮▮▮–▮▮▮

CERAMICS INTERNATIONAL

www.elsevier.com/locate/ceramint

Design and self-assembly of metal-organic framework-derived porous Co_3O_4 hierarchical structures for lithium-ion batteries

Longmei Zhang[a], Bo Yan[a], Junhao Zhang[a,c], Yuanjun Liu[a], Aihua Yuan[a,*], Gang Yang[b,**]

[a]School of Environmental and Chemical Engineering, Jiangsu University of Science and Technology, Zhenjiang, Jiangsu 212003, China
[b]Jiangsu Laboratory of Advanced Functional Materials, Department of Chemistry,Changshu Institute of Technology, Changshu 215500, China
[c]State key Laboratory of Fire Science, University of Science and Technology of China, Hefei 230027, China

Received 2 October 2015; received in revised form 20 November 2015; accepted 7 December 2015

Abstract

Porous metal oxides hierarchical structures with controlled morphologies have received great attention because of their promising applications in catalysis, energy storage, gas sensing, etc. Porous Co_3O_4 hierarchical structures with controlled morphologies were synthesized on the basis of a pyrolytic conversion of Co-based metal-organic frameworks (Co-MOFs), which were initially grown in solutions containing $Co(NO_3)_2 \cdot 6H_2O$, 1,3,5-Benzentricarboxylic acid and pyrazine as solute and N,N-dimethylformamide (DMF) as solvent under a solvothermal condition. Porous Co_3O_4 with twin hemispherical and flower-like structures were obtained with the assistance of PVP by adjusting the amount of pyrazine. The results of nitrogen adsorption–desorption indicate the BET surface area (22.6 $m^2\ g^{-1}$) of twin hemispherical Co_3O_4 structures is lower than that (33.3 $m^2\ g^{-1}$) of flower-like Co_3O_4 structures. However, the pore size of twin hemispherical Co_3O_4 structures is smaller, which is centered at about 2.5, 4.0 and 20.0 nm. The Co_3O_4 with twin hemispherical structures exhibit more excellent electrochemical performance as anode materials for lithium ion batteries than that of flower-like Co_3O_4 structures, which may be attributed to the smaller particle size and compact porous structures with suitable pore size.

Keywords: MOF; Co_3O_4; Anode materials; Scanning electron microscopy; Lithium-ion batteries

1. Introduction

Hierarchical micro- and nanostructures of porous metal oxides have attracted considerable attention due to their highly ordered architectures and well-defined physical properties, which show various potential applications in energy storage and conversion, adsorption, catalysis, gas sensing, etc. [1–4]. In past decades, tremendous efforts have been devoted to synthesize porous hierarchical structures involving the coating of a shell on removable or sacrificial templates based on different principles including the galvanic replacement [5,6], Kirkendall effect [7,8], ionic exchange [9,10], chemical etching [11,12], self-assembly [13], thermal decomposition [14,15], etc. Among the diverse synthetic methods, the self-sacrificial template strategy based on thermolysis of solid precursors is considered to be the most straightforward and representative one in fabricating porous hierarchical structures due to its low cost and effectiveness. For instance, 3D flower-like Co_3O_4 hierarchical microstructures were assembled by hexagonal porous nanoplates using facile surfactant-free hydrothermal and annealing processes [16]. Hierarchical porous $ZnCo_2O_4$ microspheres were successfully synthesized via a solvothermal method followed by an annealing process [17]. Hierarchical porous NiO nanoflowers were converted from flower-like α-$Ni(OH)_2$ nanostructures through calcinations procedure [18]. The design of novel and complex porous metal oxides hierarchical structures by a simple, low cost and

*Corresponding author. Tel.: +86 511 85639001; fax: +86 511 85635850.
**Corresponding author.
E-mail addresses: aihua.yuan@just.edu.cn (A. Yuan), gyang@cslg.edu.cn (G. Yang).

http://dx.doi.org/10.1016/j.ceramint.2015.12.038
0272-8842/

Please cite this article as: L. Zhang, et al., Design and self-assembly of metal-organic framework-derived porous Co_3O_4 hierarchical structures for lithium-ion batteries, Ceramics International (2015), http://dx.doi.org/10.1016/j.ceramint.2015.12.038

effective method is still a very interesting topic in the field of advanced materials science, although it has been studied extensively.

Recently, metal-organic frameworks (MOFs) as sacrificial templates were devised to fabricate porous metal oxides or carbon nanostructures through thermal decomposition under controlled atmospheres [19–23]. MOFs are a class of organic–inorganic hybrid functional materials with high porosity and large specific surface area. It's worthwhile to note that their pore sizes and morphologies can be easily tuned upon the selection of different metal ions and organic bridging ligands, and the porosity and long-range ordering of MOFs can offer a fast and convenient access to income and leave small molecules and ions in the transformation process. Recently, research emphasizing tuning and controlling of MOF crystal morphology and size becomes a newer way of tailoring MOF properties for specific functions, such as gas storage [24,25] and biomedical imaging [26].

Porous structures have been proven to have appropriate Li-ion diffusion lengths and large contact area with electrolytes [27,28]. Poizot et al. suggested that there are optimum particle and pore size of each metal oxide for the best electrochemical performance [29]. Co_3O_4 has been widely applied electrode materials in supercapacitors and lithium-ion battery [30]. Admittedly, specific surface areas of the obtained porous Co_3O_4 products are remarkably enlarged relative to solid particles. However, some formed porous Co_3O_4 products failed to maintain original morphologies of the precursor templates, probably due to a lack of suitable templates or optimal synthetic conditions. So it still remains a great challenge to synthesize porous Co_3O_4 with specific morphology and high specific surface area. In this study, Co-MOFs have been selected as a model MOFs to investigate the feasibility of MOFs as sacrificial templates for large-scale controllable preparation of porous metal oxides hierarchical structures. By controlling the reaction parameters, twin hemispherical and flower-like Co-MOFs hierarchical structures were synthesized and calcined to obtain porous Co_3O_4 hierarchical structures with corresponding morphologies at 500 °C for 30 min under air atmosphere. The results indicate that twin hemispherical Co_3O_4 hierarchical structures with smaller pore and particle size display excellent reversible capacity and good cycle performance, and the initial discharge capacity is as high as 1325.5 mA h g^{-1}.

2. Experimental procedure

2.1. Synthesis of Co-based metal-organic frameworks (Co-MOFs)

2.1.1. Synthesis of twin hemispherical Co-MOFs

In a typical solvothermal preparation procedure, 0.5 mmol cobalt nitrate hexahydrate, 0.5 mmol 1,3,5-Benzentricarboxylic acid, 0.9 mmol pyrazine and 1.31 g PVP (K85–95) were dissolved in 30 mL DMF. After magnetically stirred for 10 min, the homogeneous solution was transferred into a Teflon-lined stainless steel autoclave with 40 mL capacity, and placed in an oven at 150 °C for 24 h. Finally, the resulting purple powders were collected by centrifugation and washed with ethanol for 3 times and dried at 60 °C in a vacuum oven for 6 h. The prepared sample was designated as Co-MOFs-a.

2.1.2. Synthesis of novel flower-like Co-MOFs

The preparation procedure of the novel flower-like Co-MOFs was similar to that of the twin hemispherical Co-MOFs, which only changed the amount of pyrazine from 0.9 to 3 mmol. Finally, the light purple products were obtained, which were designated as Co-MOFs-b.

2.2. Synthesis of porous Co_3O_4 hierarchical structures

The above-synthesized Co-MOFs precursors were put into a ceramic crucible and then heated to 500 °C with a heating rate 1 °C min^{-1}, and maintained at 500 °C for 30 min under air atmosphere. The Co-MOFs-a and Co-MOFs-b were finally converted into two fluffy black powders, which were designated as Co_3O_4-a and Co_3O_4-b, respectively.

2.3. Characterization

2.3.1. Characterization of materials

Thermogravimetric analysis (TGA) of the Co-MOFs precursors were carried out on a Rigaku standard TG-DTG analyzer under air atmosphere in the temperature range of 25–550 °C with a heating rate of 15 °C min^{-1}. FTIR spectra of KBr powder pressed pellets were recorded on a Bruker Vector 22 spectrometer. X-ray powder diffraction (XRD) patterns were recorded on a MAX-RB X-ray diffractometer (Rigaku, Japan) equipped with graphite-monochromatized Cu Kα radiation ($\lambda = 1.54178$ Å). The field-emission scanning electron microscopy (FESEM) images of the products were taken by using a field-emission scanning electron microscope (FESEM, JEOL JSM-7600F) and transmission electron microscope (TEM) and high-resolution TEM (HRTEM) images were taken on a JEM-2100F high-resolution transmission electron microscope at an acceleration voltage of 200 kV. Energy-dispersive X-ray (EDX) analysis was performed for the products using the energy-dispersive X-ray spectroscopy attached to the JSM-6700F. X-ray photoelectron spectroscopy (XPS) of the products was performed on a Perkin-Elmer model PHI 5600 system with a monochromatic Kα radiation (1486.6 eV) X-ray source. The nitrogen adsorption–desorption isotherms and textural properties were determined on a Micromeritics Instrument Corporation sorption analyzer (TriStar II 3020).

2.3.2. Characterization of electrochemical performance

The electrochemical performance of Co_3O_4 after calcination was carried out using a coin cell (CR2016). The working electrodes consist of 70 wt% active materials (Co_3O_4-a or Co_3O_4-b), 20 wt% of conductivity agent (Super P) and 10 wt% of polymer binder (polyvinylidene fluoride, PVDF) mixed with N-methyl-2-pyrrolidone (NMP). After being stirred for 2 h, the slurry was pasted on a Cu foil using a doctor blade, and dried

Please cite this article as: L. Zhang, et al., Design and self-assembly of metal-organic framework-derived porous Co_3O_4 hierarchical structures for lithium-ion batteries, Ceramics International (2015), http://dx.doi.org/10.1016/j.ceramint.2015.12.038

at 120 °C for 12 h under vacuum to serve as the working electrode. The coin cells were assembled in an argon-filled glove box using lithium as the negative electrodes, Celgard 2500 as the separators, and 1 mol L^{-1} $LiPF_6$ (dissolved in ethylene carbonate, dimethyl carbonate and ethyl methyl carbonate, with a 1:1:1 volume ratio) as the electrolytes. The galvanostatic charge and discharge tests were performed between 0.01 and 3.0 V at different current density on battery testing system (LAND CT2001A, Wuhan, China). Cyclic voltammetry (CV) measurements were carried out on a PARSTAT2273 electrochemical workstation (Princeton Applied Research, USA) at a scanning rate of 0.1 mV s^{-1} in the potential range of 0–3 V. Electrochemical impedance spectroscopy (EIS) was performed using PARSTAT2273 electrochemical workstation; the sinusoidal excitation voltage applied to the cells was kept at 5 mV and with a frequency range of 100 kHz to 10 mHz.

3. Results and discussion

3.1. Morphological and structural characterization

To control the morphologies of porous Co_3O_4 hierarchical structures after thermal decomposition of Co-MOFs, cobalt complexes with the ligands of 1,3,5-benzentricarboxylic acid and pyrazine were synthesized, and different morphologies of Co-MOFs (Co-MOFs-a and Co-MOFs-b) were controlled by adjusting the amount of pyrazine. In order to understand the morphologies and structures of Co-MOFs, FESEM was employed to investigate the structures and morphologies of Co-MOFs-a and Co-MOFs-b in Fig. 1, which indicate that both Co-MOFs-a and Co-MOFs-b have uniformed morphologies with hierarchical structures. It is noteworthy that the Co-MOFs-a displays twin hemispherical structures with the average size of 2 μm, and the equatorial juncture between the crystal halves can be clearly observed from the FESEM image in Fig. 1(a). The high magnification FESEM image in Fig. 1(b) reveals that the large configuration assembled by small nanocrystals with the size of less 100 nm. When the amount of pyrazine is increased to 3 mmol from 0.9 mmol, Fig. 1(c) shows that Co-MOFs-b is relatively uniform flower-like structures, which is self-assembled by nanosheets. From the high magnification image in Fig. 1(d), the diameter of these novel flower-like structures is from 10 to 15 μm, and the thickness of nanosheets is about 50 nm.

The Fourier transform infrared (FTIR) spectrum of 1,3,5-benzentricarboxylic acid, pyrazine, Co-MOFs-a and Co-MOFs-b were measured at room temperature for elucidating the structures and components of the Co-MOFs, as shown in Fig. 2(a). The strong peak around 1720 cm^{-1} is assigned to C=O stretching vibration, and the characteristic peaks at 1606, 1454 and 1404 cm^{-1} are attributed to the antisymmetric

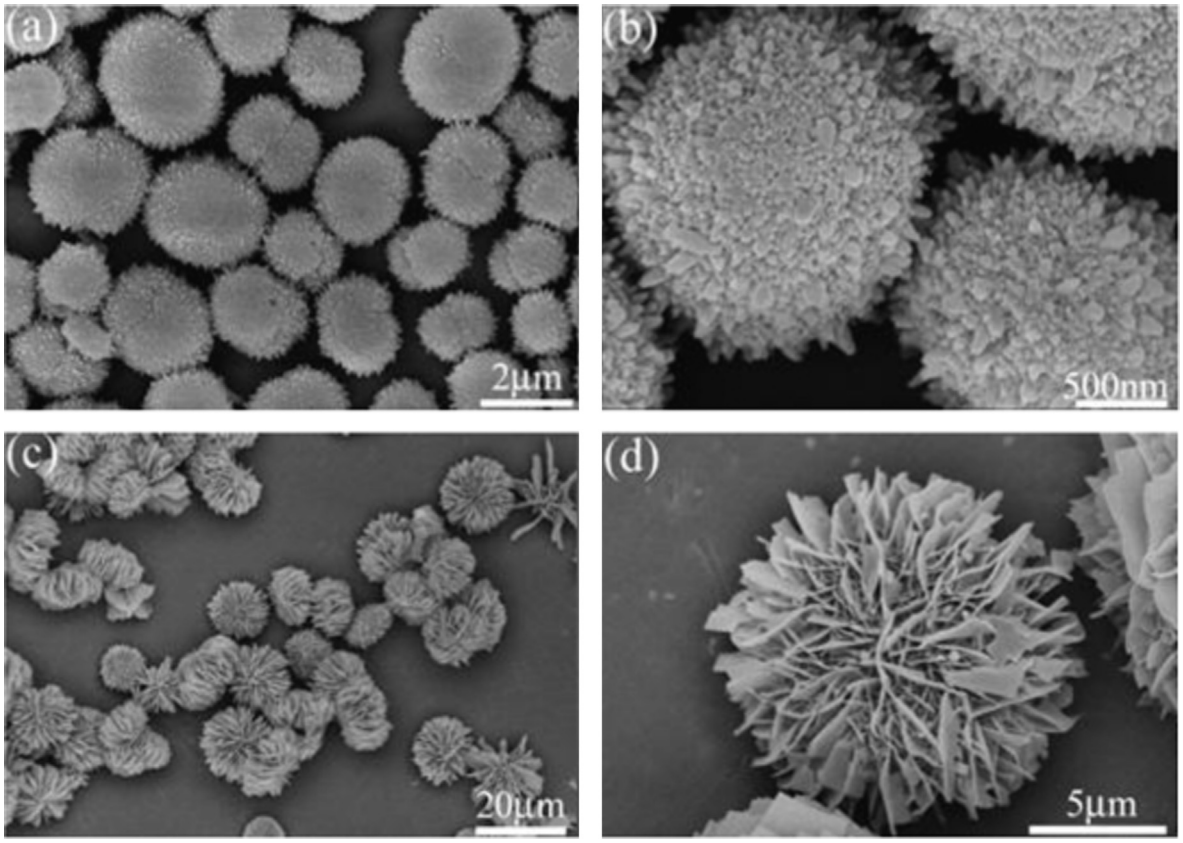

Fig. 1. (a) and (b) Different magnification FESEM images of Co-MOFs-a; (c) and (d) different magnification FESEM images of Co-MOFs-b.

Please cite this article as: L. Zhang, et al., Design and self-assembly of metal-organic framework-derived porous Co_3O_4 hierarchical structures for lithium-ion batteries, Ceramics International (2015), http://dx.doi.org/10.1016/j.ceramint.2015.12.038

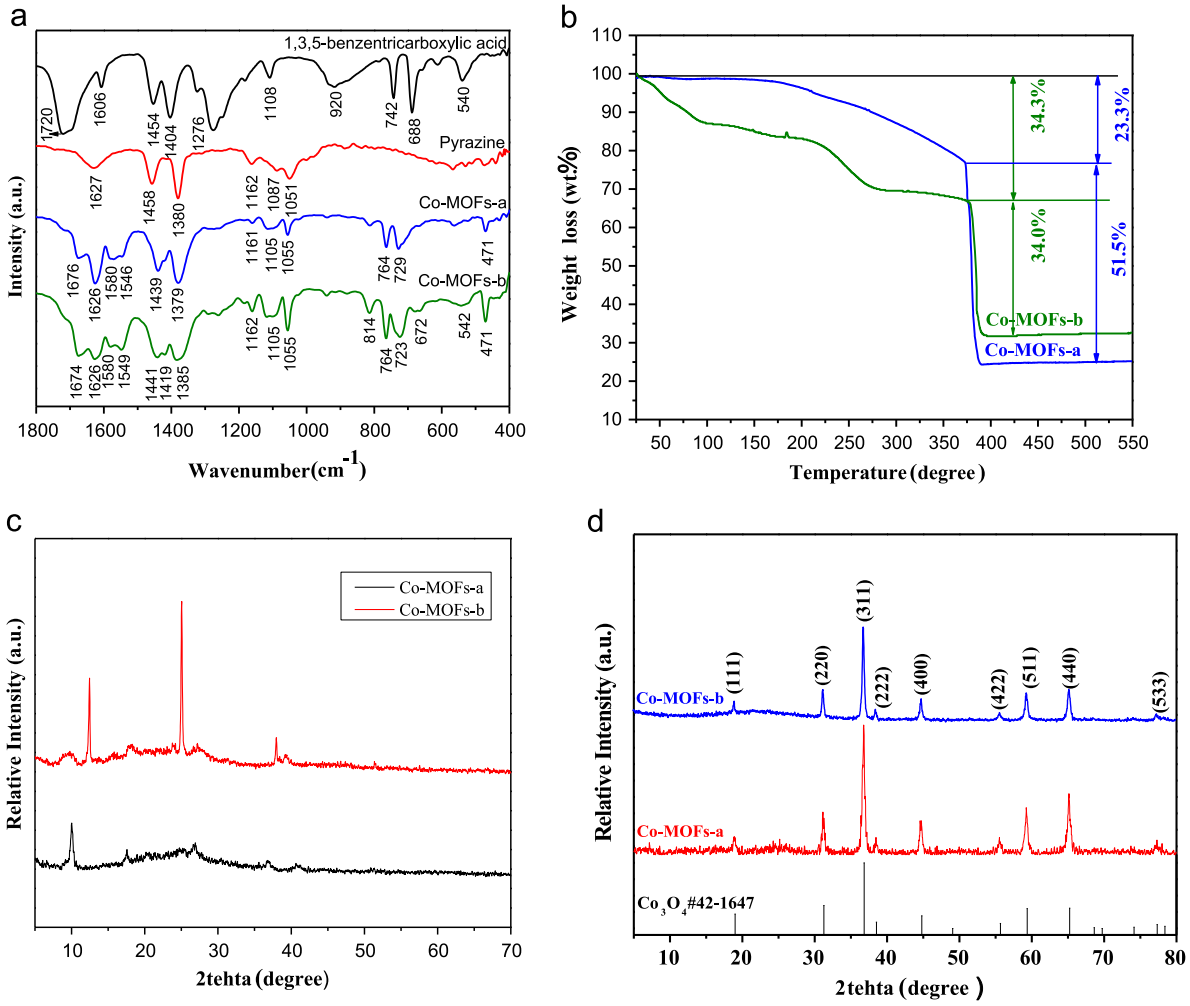

Fig. 2. (a) XRD patterns of Co_3O_4-a, Co_3O_4-b and the standard data of Co_3O_4 from JCPDS card no. 42-1467; (b) TGA curves of Co-MOFs-a and Co-MOFs-b in air atmosphere at a heating rate of 15 °C min^{-1}; (c) FTIR spectra of 1,3,5-benzentricarboxylic acid, pyrazine, Co-MOFs-a, and Co-MOFs-b; (d) XRD patterns of Co-MOFs-a and Co-MOFs-b.

stretching vibration and symmetric stretching vibrations of the COO^- of 1,3,5-benzentricarboxylic acid. In the FTIR spectra of Co-MOFs-a and Co-MOFs-b, absorption bands at about 1720 cm^{-1} is disappeared, which is attributed to the deprotonation of 1,3,5-benzentricarboxylic acid due to the reaction with the metal ions [31]. The stretching vibration and symmetric stretching vibration peaks of the COO^- for Co-MOFs-a and Co-MOFs-b are moved to 1546 or 1549 cm^{-1}, 1439 or 1441 cm^{-1}, 1379 or 1385 cm^{-1}, which indicate that the chelating or bridge bidentate have been formed between COO^- and Co^{2+}. In the FTIR spectra of pyrazine, the peak at 1627 cm^{-1} is due to C=N stretching vibration. After the formation of complexes, the peaks at about 1580 cm^{-1} are also ascribed to C=N stretching vibration which indicate that the two nitrogen atoms of pyrazine and cobalt ions formed coordination bonds. Therefore, it is believed that Co-MOFs-a and Co-MOFs-b might be Cobalt complexes with the ligands of 1,3,5-benzentricarboxylic acid and pyrazine after solvothermal treatment.

TGA of the Co-MOFs-a and Co-MOFs-b was carried out in air atmosphere to measure the weight loss occurring during pyrolysis, which is shown in Fig. 2(b). The results indicate that the weight loss of Co-MOFs-a includes a slow weight loss (23.3%) from 20 to 375 °C and a fast weight loss (51.5%) from 375 to 388 °C. Little weight loss befor 150 °C indicates that there are little amount of crystal water in Co-MOFs-a. The weight loss from 150 °C to 375 °C is attributed to the release of DMF. From 375 to 388 °C, the weight loss can be ascribed to the decomposition of complex and subsequent oxidation of ligands. However, the weight loss of Co-MOFs-b may be divided four parts. The weight loss (12.9%) before 100 °C is the desorption of crystal water, and the weight loss (3.9%) from 100 to 200 °C is mainly attributed to the release of coordinated water; and the weight loss (34.0%) from 200 to 283 °C is ascribled to the removal of DMF. From 375 to 393 °C, the weight loss can be attributed to the decomposition of complex and subsequent oxidation of ligands. The above results indicate that Co-MOFs-b has higher porosity. The residual weight ratio of Co-MOFs-b is higher than that of Co-MOFs-a, which might be due to the fact that the numbers of 1,3,5-benzentricarboxylic acid and pyrazine ligands are different in Co-MOFs-a and Co-MOFs-b. The XRD results

Please cite this article as: L. Zhang, et al., Design and self-assembly of metal-organic framework-derived porous Co_3O_4 hierarchical structures for lithium-ion batteries, Ceramics International (2015), http://dx.doi.org/10.1016/j.ceramint.2015.12.038

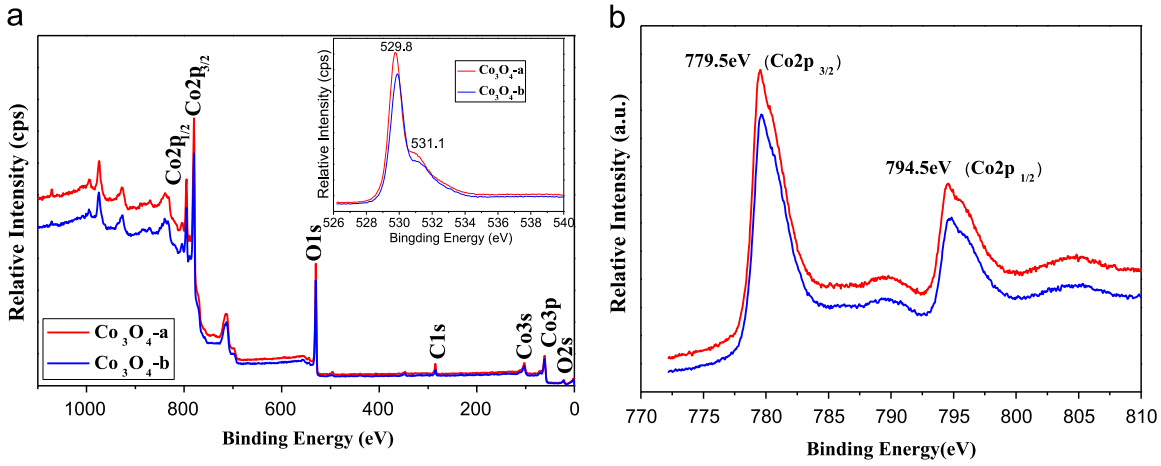

Fig.3. XPS spectra of Co_3O_4-a and Co_3O_4-b: (a) full survey scan spectrum and O1s peak in the inset; (b) Co2p peaks.

in Fig. 2(c) also prove that Co-MOFs-a and Co-MOFs-b are different complexes although no standard PDF cards match with the XRD pattern of Co-MOFs-a and Co-MOFs-b. With increasing the thermal decomposition temperature, there are no remarkable weight losses beyond 393 °C, indicating that Co-MOFs have decomposed completely. Hence, in order to yield pure and high crystalline Co_3O_4 phase, Co-MOFs were calcined at 500 °C for 30 min.

By calcining the Co-MOFs precursors at 500 °C for 30 min in air, fluffy black powders (Co_3O_4-a and Co_3O_4-b) were obtained. To ascertain the components and structures of the products after calcination, Fig. 2(d) shows the XRD patterns to investigate the crystal phases of Co_3O_4-a, Co_3O_4-b. All the diffraction peaks of Co_3O_4-a and Co_3O_4-b can be readily indexed to *f.c.c* phase Co_3O_4 (JCPDS card no. 42-1467). No other impurity peaks are detected such as CoO and Co_2O_3, revealing that the Co-MOFs precursors were converted to crystalline Co_3O_4 completely. Additionally, all the diffraction peaks of Co_3O_4-a and Co_3O_4-b are significantly broaden in width and weaken in intensity, which suggests that the as-obtained Co_3O_4 are essentially constructed with a large number of nanosized crystallites.

X-ray photoelectron spectra (XPS) have often been used for surface characterization of various materials, and unambiguous results are readily obtained when the various surface components each contain unique elemental markers. Here, in order to analyze the surface component of Co_3O_4-a and Co_3O_4-b, XPS of the products were measured, which are shown in Fig. 3. It can be found that the peaks on the full patterns are mainly attributed to C1s (285.6 eV), O1s (529.2 eV) and Co2p (794.5 and 779.5 eV) and their corresponding Auger peaks in Fig. 3a, indicating the existence of carbon, oxygen, and cobalt element. However, the lower peak for C1s binding energy suggests that the products consist of C elements, which is from a small amount of residue of the decomposition of organic ligands. Additionally, it is also found that the Co2p and O1s XPS peaks of the two Co_3O_4 samples are analogous for their position and intensity. Fig. 3(b) shows that the Co2p XPS spectra present two major peaks at 794.5 and 779.5 eV, which can be attributed to $Co2p_{1/2}$ and $Co2p_{3/2}$ of the Co_3O_4-a and Co_3O_4-b. The absence of prominent shakeup satellite peaks in the Co2p spectra further indicates the formation of the Co_3O_4 phase. The deconvoluted O1s spectrum in the inset of Fig. 3(a) exhibit two peaks at 529.8 and 531.1 eV, which can be assigned to the lattice oxygen of spinel Co_3O_4 [32]. The XPS results further prove that the as-synthesized products are Co_3O_4.

In order to investigate the effect of Co-MOFs as sacrificial templates for the morphologies of the products, FESEM were employed to measure the morphologies and structures of Co_3O_4-a and Co_3O_4-b. Typical morphologies are shown in Fig. 4(a) and (b). Obviously, the calcined products retain the similar sizes and shapes of the Co-MOFs-a and Co-MOFs-b precursors. Fig. 4(a) shows that Co_3O_4-a is sphere-like shape, which is assembled by many uniform nanoparticles with the diameter of about 50 nm. Fig. 4(b) displays that Co_3O_4-b is still flower-like shape by assembly of nanosheets, and the inset of Fig. 4(b) reveals that the surface of nanosheets becomes fairly rough compared to the nanosheets of Co-MOFs precursors, and the rough nanosheets are assembled by smaller nanoparticles which is less than 100 nm. The EDX spectrum in Fig. 4(c) and (d) further confirm that the two samples all contain Co and O elements, and no other elements are detected, which are consistent with the results of XRD. The results provide an efficient way to facilitate the formation of the tunable morphologies of Co_3O_4.

More structural information of Co_3O_4-a and Co_3O_4-b were investigated by TEM and HRTEM characterization. As shown in Fig. 5(a), the projection profile of Co_3O_4-a remains twin hemispherical shape, agreeing well with the morphology in the FESEM observation. The high magnification TEM image in Fig. 5(b) shows the Co_3O_4 twin hemispherical architecture is porous structure, which is composed of numerous nanoparticles. The reason may be the successive release and loss of CO_2, N_xO_y and H_2O during the thermal decomposition of precursors. The TEM image of scattered nanoparticles in the inset of Fig. 5(b) indicates that the size of nanoparticles is from 23 to 45 nm. As evidence, the HRTEM image (Fig. 5(c)) shows that these nanoparticles are attached with each other in various orientations, despite displaying clear lattice fringes

Please cite this article as: L. Zhang, et al., Design and self-assembly of metal-organic framework-derived porous Co_3O_4 hierarchical structures for lithium-ion batteries, Ceramics International (2015), http://dx.doi.org/10.1016/j.ceramint.2015.12.038

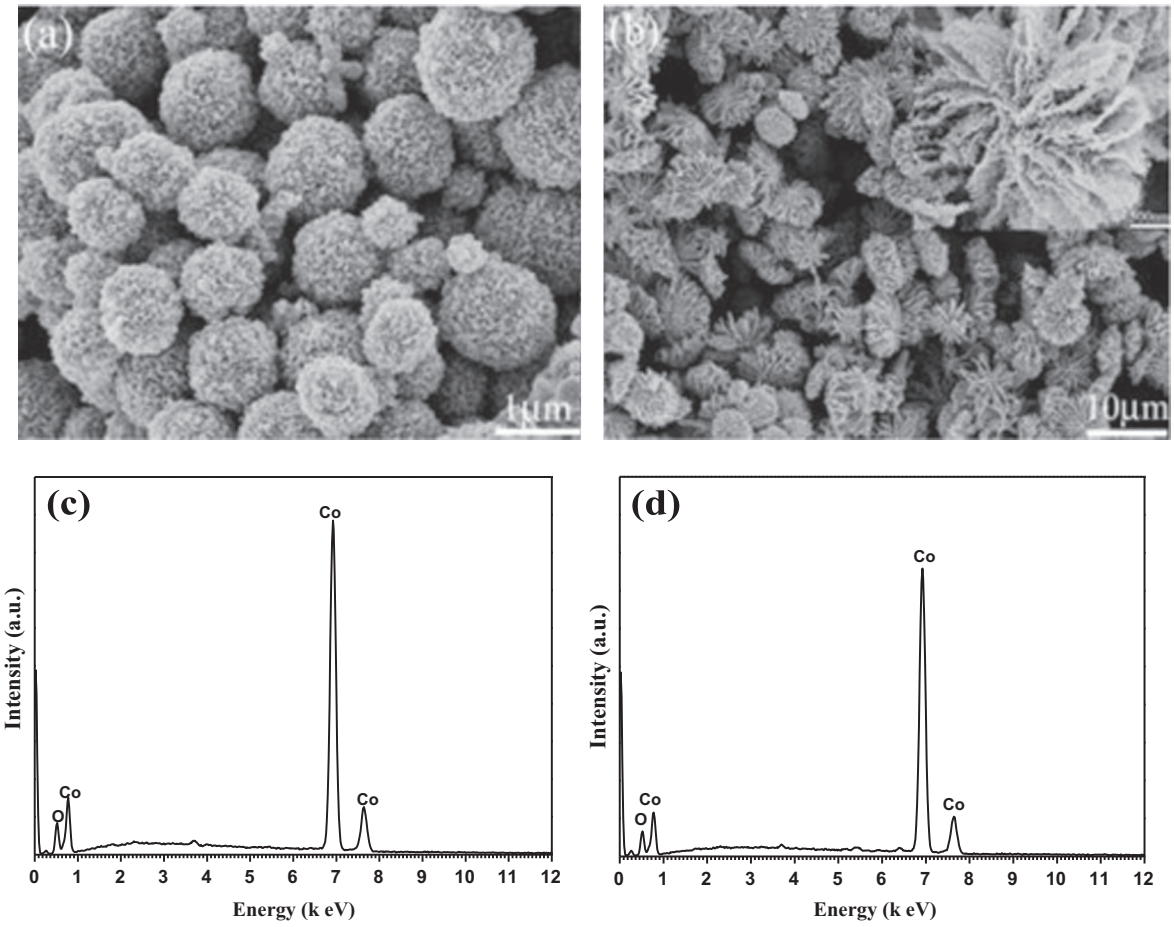

Fig. 4. (a) FESEM images of Co_3O_4-a; (b) FESEM images of Co_3O_4-b; (c) EDX spectrum of Co_3O_4-a; (d) EDX spectrum of Co_3O_4-b.

with spacings of 0.46 nm and 0.24 nm, which correspond to the (220) and (311) planes, respectively. The selected area electronic diffraction (SAED) pattern recorded from the whole twin hemispherical architecture (inset of Fig. 5(c)) shows a series of concentric rings, indicating the twin hemispherical architecture is polycrystalline structure. Fig. 5(d) displays individual flower-like structure with the diameter of 8 μm. The high magnification TEM image in Fig. 5(e) shows that the nanosheets are porous structures which are assembled by nanoparticles. The sizes of particles are between 50 and 100 nm. The HRTEM image also displays clear lattice fringes with spacings of 0.46 nm and 0.24 nm in Fig. 5(f), which correspond to the (220) and (311) planes. The SAED pattern from the nanosheets (inset of Fig. 5(f)) shows a series of concentric rings, indicating the nanosheets are polycrystalline structures.

Nitrogen absorption–desorption isotherms were performed to obtain information about the specific surface areas and pore sizes of the calcined samples at 77 K. Fig. 6(a) and (c) indicates that Co_3O_4-a and Co_3O_4-b display typical IV adsorption–desorption isotherms with distinct hysteresis loop at a relative pressures of 0.68–1.0 and 0.79–1.0, respectively, which suggest the presence of mesoporous structures [33]. The Brunauer–Emmett–Teller (BET) specific surface area of Co_3O_4-a and Co_3O_4-b were calculated to be 22.6, 33.3 $m^2\ g^{-1}$, respectively. The pore size distribution derived from the adsorption branch using the BJH method shows that the pore size of Co_3O_4-a is centered at about 2.5, 4.0 and 20.0 nm in Fig. 6(b), and the pore size of Co_3O_4-b is centered at about 2.45 and 21.0 nm in Fig. 6(d). According to the morphology and structure characteristic, the pore structures can be attributed to the decomposition process that the ligands were removed and resulted in the formation of small pores.

3.2. Electrochemical performances

Such porous Co_3O_4 hierarchical structures can not only shorten diffusion length for Li^+, but also provide adequate buffer space for volume expansion to enhance lithium performance during the cycling process [34]. In order to prove the applicability of the porous Co_3O_4 hierarchical structures in lithium ion batteries, the electrochemical properties with respect to Li insertion/extraction were investigated, as shown in Fig. 7. In the charge–discharge curves of Co_3O_4-a and Co_3O_4-b in the voltage of 0.001–3.0 V (vs. Li^+/Li) at a constant current density of 100 mA g^{-1} at ambient temperature in Fig. 7(a) and (b), it can be clearly seen that there are two potential plateaus which is similar to the previous report [35]. As shown in Fig. 7(a), the initial discharge capacity of Co_3O_4-a is as high as 1325.5 mA h g^{-1}, which is higher than

Please cite this article as: L. Zhang, et al., Design and self-assembly of metal-organic framework-derived porous Co_3O_4 hierarchical structures for lithium-ion batteries, Ceramics International (2015), http://dx.doi.org/10.1016/j.ceramint.2015.12.038

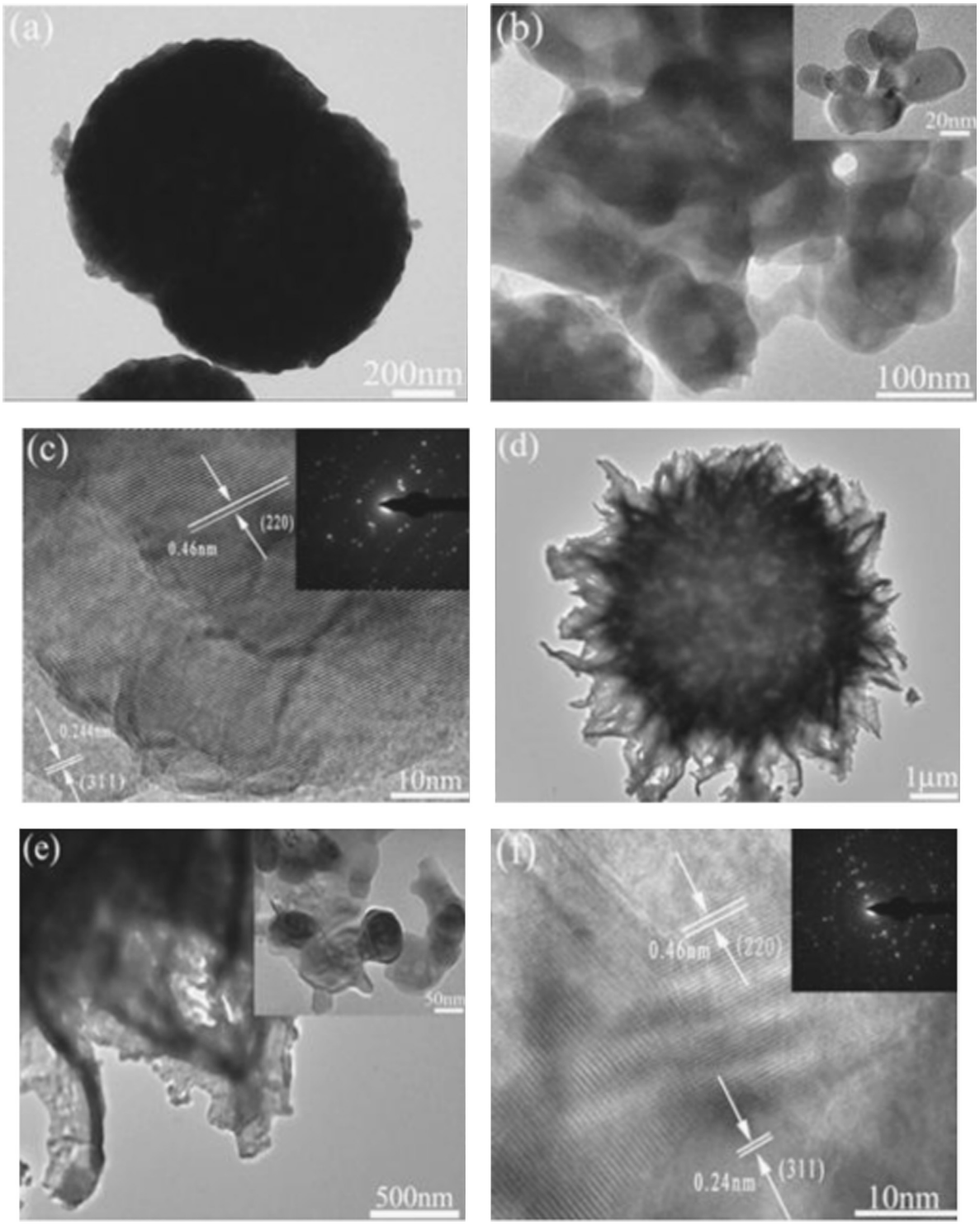

Fig. 5. (a) Low-magnification TEM image of the Co_3O_4-a; (b) high-magnification TEM image of Co_3O_4-a; (c) HRTEM image of the Co_3O_4-a, and the inset is the SAED pattern; (d) low magnification TEM image of Co_3O_4-b; (e) high-magnification TEM image of Co_3O_4-b; (f) HRTEM image of the Co_3O_4-b, and the inset is the SAED pattern.

the theoretical capacity (890 mA h g^{-1}). The first charge capacity is approximate 1003.5 mA h g^{-1}, and the coulombic efficiency is about 75.7%. The irreversible capacity in the first cycle is usually ascribed to the decomposition of the electrolyte to form SEI layers and interfacial lithium storage, which is common for most anode materials [36]. The reversible capacities of the electrode in the 2nd, 5th and 10th cycles are about 965 mA h g^{-1}, 840.6 mA h g^{-1}, 749 mA h g^{-1}, respectively, and the coulombic efficiencies are all above 1, which indicate that the porous hierarchical Co_3O_4-a electrode has a much higher capacity as well as good capacity retention. Furthermore, its columbic efficiencies of Co_3O_4-a and

Please cite this article as: L. Zhang, et al., Design and self-assembly of metal-organic framework-derived porous Co_3O_4 hierarchical structures for lithium-ion batteries, Ceramics International (2015), http://dx.doi.org/10.1016/j.ceramint.2015.12.038

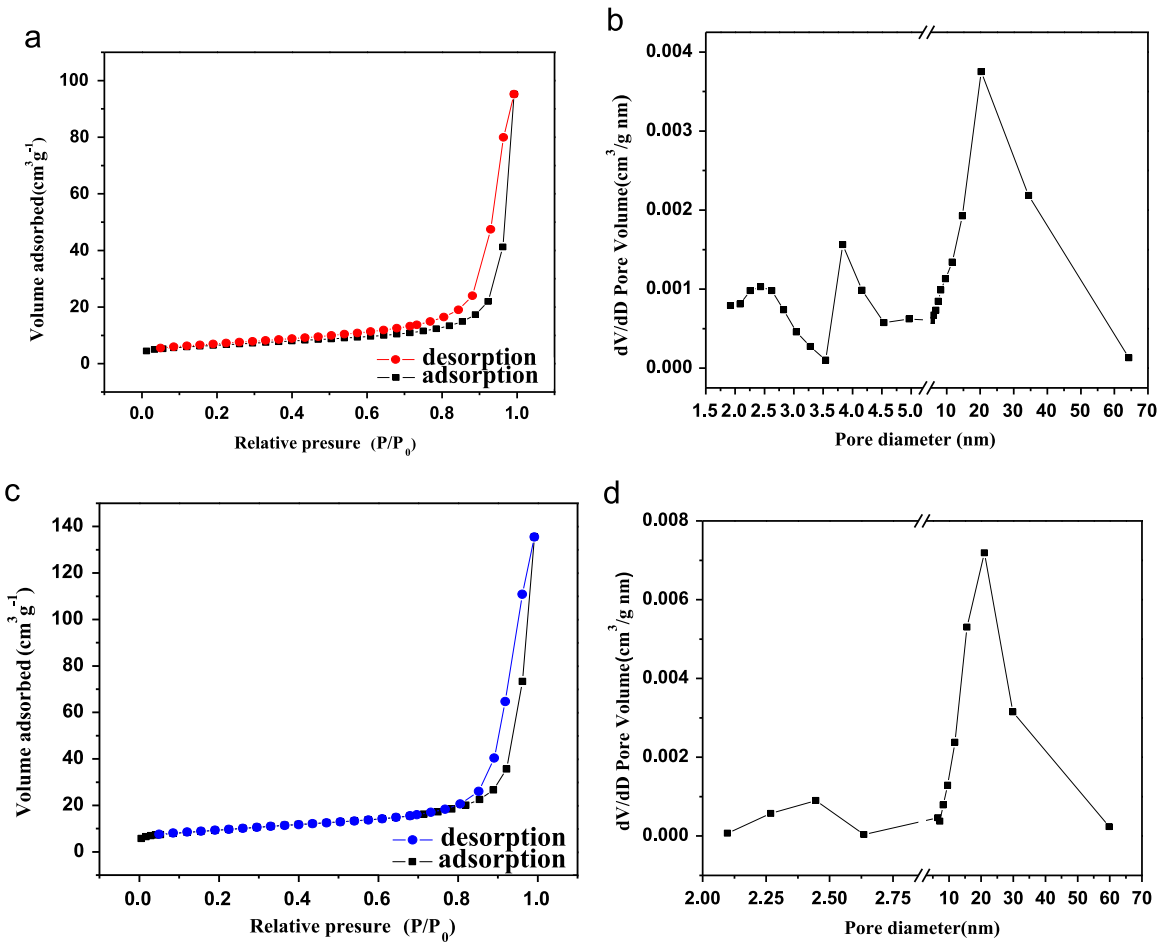

Fig. 6. (a) N_2 adsorption desorption isotherms of Co_3O_4-a; (b) N_2 adsorption desorption isotherms of Co_3O_4-b; (c) pore size distribution of Co_3O_4-a; (d) pore size distribution of Co_3O_4-b.

Co_3O_4-b are almost all above 100% except for the first charge–discharge cycles. It might be due to the fact that in the discharge process more Li involve in the active material of Co_3O_4, but in the charge process not all of Li are removed from Co_3O_4. The minor irreversibility of active material results in the columbic efficiencies of both samples higher than 1. Compared with the twin hemispherical porous Co_3O_4 structures, the flower-like porous Co_3O_4 structures (Co_3O_4-b) hinder more lithium cations to involve in the lithiation/delithiation processes of Co_3O_4, and present relatively low capacities in Fig. 7(b). Therefore, the morphology and structure of Co_3O_4 play crucial roles in the high performance anode materials for lithium batteries. The cycling performances of Co_3O_4-a and Co_3O_4-b at a current density of 100 mA g^{-1} are shown in Fig. 7(c). The capacities of the Co_3O_4-a and Co_3O_4-b electrodes achieved a maximum initial capacities of 1325.5 and 1243 mA h g^{-1}, respectively. After 90 cycles, the reversible capacity of Co_3O_4-a retains 470.3 mA h g^{-1}, which is lower than the value (529.2 mA h g^{-1}) of Co_3O_4-b capacity. Even so, the values are all higher than the commercial graphite anode (372 mA h g^{-1}). The excellent performance of porous Co_3O_4 hierarchical structures are probably attributed to that the small nanoparticle subunits and porous structures facilitate the electrolyte penetration and Li^+ ions transport in the electrode and the hierarchical porous structures could efficiently buffer the stress caused by the volume variation during the charge–discharge process. Notably, twin hemispheric porous Co_3O_4 structures show better capacity retention and stability due to the maximization of the beneficial effects arising from the compact porous hierarchical structures, which could better withstand the repeated volume expansion/contraction and facilitate the lithium ions insertion with reduced diffusion length [37].

To understand the eletrochemical performances, the cyclic voltammograms (CV) measurements were performed on Co_3O_4-a and Co_3O_4-b electrodes to characterize their electrochemical reactions in Li ion batteries. Fig. 8 shows the first three consecutive CV curves of the electrodes made from Co_3O_4-a and Co_3O_4-b recorded between 5 mV and 3 V at a scan rate of 0.1 mV s^{-1}. In the first cycle, the cathodic peaks are observed at around 1.10 V for Co_3O_4-a and at 0.70 and 0.33 V for Co_3O_4-b, which can be attributed to the electrochemical reduction (lithiation) reaction of Co_3O_4 with Li and formation of partially irreversible solid electrolyte interface (SEI) [38]. The main anodic peaks are observed at 2.10 V for Co_3O_4-a and at 1.64 V for Co_3O_4-b, which could be ascribed to the oxidation of CoO to Co^{3+}. Compared to the first cycle, the peak intensity and integral areas of the second and third

Please cite this article as: L. Zhang, et al., Design and self-assembly of metal-organic framework-derived porous Co_3O_4 hierarchical structures for lithium-ion batteries, Ceramics International (2015), http://dx.doi.org/10.1016/j.ceramint.2015.12.038

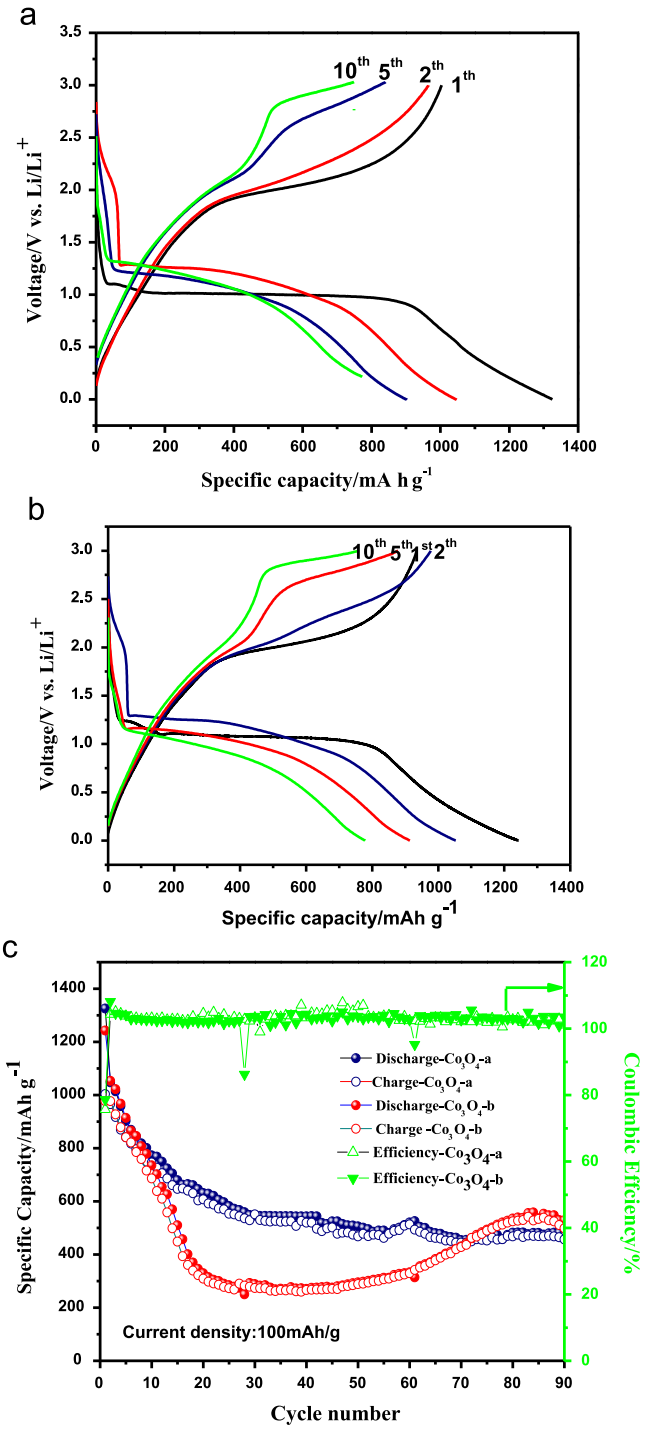

Fig.7. (a) Charge–discharge curves of Co_3O_4-a at a current rate of 100 mA g^{-1}; (b) charge–discharge curves of Co_3O_4-b at a current rate of 100 mA g^{-1}; (c) cycling performance of Co_3O_4-a and Co_3O_4-b at a current rate of 100 mA g^{-1}.

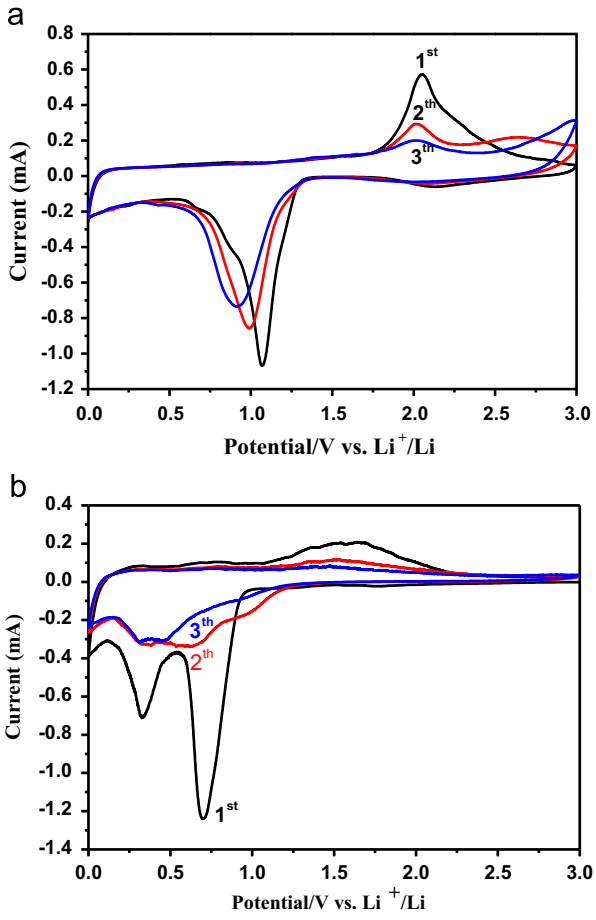

Fig. 8. Cyclic voltammogram curves scanned at a rate of 0.1 mV s^{-1}: (a) of Co_3O_4-a; (b) of Co_3O_4-b.

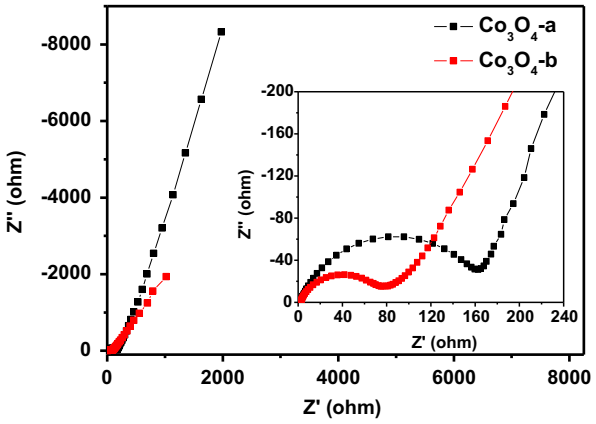

Fig. 9. Nyquist plots of Co_3O_4-a and Co_3O_4-b anode materials.

cycles are reduced for Co_3O_4-a but are decreased more obviously for Co_3O_4-b, which indicate that the electrochemical reversibility of Co_3O_4-a was gradually built and highly stable SEI layer was formed after the initial cycle and much better than those for Co_3O_4-b. Additionally, cathodic peak about 1.1 V and anodic peak about 2.1 V shift to lower potential for Co_3O_4-a, which suggest drastic, lithium-driven, structural or textural modification during both the anodic and cathodic processes. Electrochemical impedance spectroscopy is carried out to identify the charge transfer resistance in the Co_3O_4-a and Co_3O_4-b electrode materials. The Nyquist plots of Co_3O_4-a and Co_3O_4-b in the frequency range from 100 kHz to 10 mHz are shown in Fig. 9. The plots consist of depressed semicircles in the high frequency regions and straight lines in the low frequency regions. Generally, the semicircle in the high frequency region represents the resistance of the lithium ion migration through the interface between the surface layer of the particles and electrolyte, while the linear region in the low

Please cite this article as: L. Zhang, et al., Design and self-assembly of metal-organic framework-derived porous Co_3O_4 hierarchical structures for lithium-ion batteries, Ceramics International (2015), http://dx.doi.org/10.1016/j.ceramint.2015.12.038

frequency region corresponds to the Warburg impedance related to the diffusion of the Li-ions in the Co_3O_4 electrodes. The inset of Fig. 9 shows that Co_3O_4-a and Co_3O_4-b have low high frequency resistance about 162 and 75 ohms, which suggests that the twin hemispherical and flower-like structures provide efficient lithium diffusion tunnels and increases the electrolyte/Co_3O_4 contact area. Based on above, it can be believed that the high capacity and good capacity retention of the Co_3O_4-a and Co_3O_4-b anode could probably be ascribed to the porous structures verified by HRTEM and BET measurements. Firstly, the small Co_3O_4 nanoparticles can shorten the diffusion length of Lithium ions insertion/extraction. Secondly, the porous structure can effectively buffer space for the volume expansion of Co_3O_4 during the cycling process so that improved the cycling stability.

4. Conclusion

A large scale and facile method was employed to synthesize Co-MOFs hierarchical structures with the assistance of PVP. Meanwhile, thermal decomposition was developed to successfully prepare intriguing twin hemispherical and novel flower-like porous Co_3O_4 hierarchical structures due to the successive release and loss of CO_2, N_xO_y and H_2O, which was assembled by many uniform nanoparticles. The results indicate that Co_3O_4-a and Co_3O_4-b remain the twin hemispherical and flower-like hierarchical structures compared with Co-MOFs-a and Co-MOFs-b, which are attributed to Co-MOFs hierarchical structures as self-sacrificial templates. Such complex hierarchical structures might bring unique physical chemistry properties. The results demonstrate that these complex hierarchical structures, especially the twin hemispheric porous Co_3O_4 hierarchical structures, exhibit remarkable electrochemical performance as anode materials for lithium ion batteries. It can be anticipated that these complex hierarchical structures would find their promising applications in many areas.

Acknowledgements

The work was financially supported by National Natural Science Foundation of China (51072072 and 51272095), Natural Science Foundation of Jiangsu Province (No. BK20141293), Natural Science Foundation of the Higher Education Institutions of Jiangsu Province (No. 13KJB430012), the Opening Project of State Key Laboratory of Fire Science (No. HZ2015-KF03), and Qing Lan Project of Jiangsu Province (No. 1614101401).

References

[1] Q.Y. An, F. Lv, Q.Q. Liu, C.H. Han, K.N. Zhao, J.Z. Sheng, Q.L. Wei, M.Y. Yan, L.Q. Mai, Amorphous vanadium oxide matrixes supporting hierarchical porous Fe_3O_4/graphene nanowires as a high-rate lithium storage anode, Nano Lett. 14 (2014) 6250–6256.

[2] J.H. Zhang, K. Yanagisawa, S.S. Yao, H. Wong, Y.S. Qiu, H.J. Zheng, Large-scale controllable preparation and performance of hierarchical nickel microstructures by seed-mediated solution hydrogen reduction route, J. Mater. Chem. A 3 (2015) 7877–7887.

[3] A.H. Yuan, H. Zhou, G.W. Diao, P.D. Southon, C.J. Kepert, L. Liu, Gas and vapor adsorption in octacyanometallate based frameworks $Mn_2[M(CN)_8]$ (M=W, Mo) with exposed Mn^{2+} sites, Int. J. Hydrog. Energy 39 (2014) 884–889.

[4] R.C. Rao, M. Yang, C.S. Li, H.Z. Dong, S. Fang, A.M. Zhang, A facile synthesis for hierarchical porous CeO_2 nanobundles and their superior catalytic performance for CO oxidation, J. Mater. Chem. A 3 (2015) 782–788.

[5] Y.G. Sun, Y.N. Xia, Shape-controlled synthesis of gold and silver nanoparticles, Science 298 (2002) 2176–2179.

[6] S.E. Skrabalak, L. Au, X.D. Li, Y.N. Xia, Facile synthesis of Ag nanocubes and Au nanocages, Nat. Protoc. 2 (2007) 2182–2190.

[7] Y.D. Yin, R.M. Rioux, C.K. Erdonmez, S. Hughes, G.A. Somorjai, A. P. Alivisatos, Formation of hollow nanocrystals through the nanoscale Kirkendall effect, Science 304 (2004) 711–714.

[8] G. Edgar, J. Arbiol, V.F. Puntes, Carving at the nanoscale: sequential galvanic exchange and Kirkendall growth at room temperature, Science 334 (2011) 1377–1380.

[9] K.S. Novoselov, A.K. Geim, S.V. Morozov, D. Jiang, Y. Zhang, S. V. Dubonos, I.V. Grigorieva, A.A. Firsov, Electric field effect in atomically thin carbon films, Science 306 (2004) 666–669.

[10] S.L. Xiong, H.C. Zeng, Serial ionic exchange for the synthesis of multishelled copper sulfide hollow spheres, Angew. Chem. Int. Ed. 51 (2012) 949–952.

[11] J.W. Park, H.M. Zheng, Y.W. Jun, A.P. Alivisatos, Hetero-epitaxial anion exchange yields single-crystalline hollow nanoparticles, J. Am. Chem. Soc. 131 (2009) 13943–13945.

[12] K.J. An, S.G. Kwon, M. Park, H.B. Na, S. Baik, J.H. Yu, D. Kim, J. S. Son, Y.W. Kim, I.C. Song, W.K. Moon, H.M. Park, T. Hyeon, Synthesis of uniform hollow oxide nanoparticles through nanoscale acid etching, Nano Lett. 8 (2008) 4252–4258.

[13] M. Hu, A.A. Belik, M. Imura, Y. Yamauchi, Tailored design of multiple nanoarchitectures in metal-cyanide hybrid coordination polymers, J. Am. Chem. Soc. 135 (2013) 384–391.

[14] J.H. Zhang, J. Du, Y.T. Qian, S.L. Xiong., Synthesis, characterization and properties of carbon nanotubes microspheres from pyrolysis of polypropylene and maleated polyprolene, Mater. Res. Bull. 45 (2010) 15–20.

[15] W. Cho, Y.H. Lee, H.J. Lee, M. Oh, Multi ball-in-ball hybrid metal oxides, Adv. Mater. 23 (2011) 1720–1723.

[16] W.Z. Wang, J. Xu, Structure and visible light luminescence of 3D flower-like Co_3O_4 hierarchical microstructures assembled by hexagonal porous nanoplates, ACS Appl. Mater. Interfaces 7 (2015) 415–421.

[17] Q.H. Wang, L.X. Zhu, L.Q. Sun, Y.C. Liu, L.F. Jiao, Facile synthesis of hierarchical porous $ZnCo_2O_4$ microspheres for high-performance supercapacitors, J. Mater. Chem. A 3 (2015) 982–985.

[18] Y. Ren, L. Gao, From three-dimensional flower-Like α-$Ni(OH)_2$ nanostructures to hierarchical porous NiO nanoflowers: microwave-assisted fabrication and supercapacitor properties, J. Am. Ceram. Soc. 93 (2010) 3560–3564.

[19] H.L. Jiang, Q. Xu, Porous metal-organic frameworks as platforms for functional applications, Chem. Commun. 47 (2011) 3351–3370.

[20] L. Zhang, H.B. Wu, S. Madhavi, H.H. Hng, X.W. (David) Lou, Formation of Fe_2O_3 microboxes with hierarchical shell structures from metal-organic frameworks and their lithium storage properties, J. Am. Chem. Soc. 134 (2012) 17388–17391.

[21] M. Hu, A.A. Belik, M. Imura, K. Mibu, Y. Tsujimoto, Y. Yamauchi, Synthesis of superparamagnetic nanoporous iron oxide particles with hollow interiors by using Prussian blue coordination polymers, Chem. Mater. 24 (2012) 2698–2707.

[22] R.B. Wu, X.K. Qian, F. Yu, H. Liu, K. Zhou, J. Wei, Y.Z. Huang, MOF-templated formation of porous CuO hollow octahedra for lithium-ion battery anode materials, J. Mater. Chem. A 1 (2013) 11126–11129.

[23] R.B. Wu, X.K. Qian, X.H. Rui, H. Liu, B. Yadian, K. Zhou, J. Wei, Q. Y. Yan, X.Q. Feng, Y. Long, L.Y. Wang, Y.Z. Huang, ZeoliticImidazolate framework 67-derived high symmetric porous Co_3O_4 hollow dodecahedra with highly enhanced lithium storage capability, Small 10 (2014) 1932–1938.

Please cite this article as: L. Zhang, et al., Design and self-assembly of metal-organic framework-derived porous Co_3O_4 hierarchical structures for lithium-ion batteries, Ceramics International (2015), http://dx.doi.org/10.1016/j.ceramint.2015.12.038

[24] H. Zhou, J. Zhang, J. Zhang, X.F. Yan, X.P. Shen, A.H. Yuan, Spillover enhanced hydrogen storage in Pt-doped MOF/graphene oxide composite produced via an impregnation method, Inorg. Chem. Commun. 54 (2015) 54–56.

[25] H. Zhou, X.Q. Liu, J. Zhang, X.F. Yan, Y.J. Liu, A.H. Yuan, Enhanced room-temperature hydrogen storage capacity in Pt-loaded graphene oxide/HKUST-1 composites, Int. J. Hydrog. Energy 39 (2014) 2160–2167.

[26] J.D. Rocca, D. Liu, W.B. Lin, Nanoscale metal-organic frameworks for biomedical imaging and drug delivery, Chem. Res. 44 (2011) 957–968.

[27] S.X. Wang, S.L. Chen, Q.L. Wei, X.K. Zhang, S.Y. Wong, S.H. Sun, X. Li, Bioinspired synthesis of hierarchical porous graphitic carbon spheres with outstanding high-rate performance in lithium-ion batteries, Chem. Mater. 27 (2015) 336–342.

[28] R.B. Wu, X.K. Qian, K. Zhou, J. Wei, J. Lou, Porous spinel $ZnxCo_{3-x}O_4$ hollow polyhedra templated for high-rate lithium-ion batteries, ACS Nano 8 (2014) 6297–6303.

[29] P. Poizot, S. Laruelle, S. Grugeon, L. Dupont, J. Tarascon, Nano-sized transition-metal oxides as negative-electrode materials for lithium-ion batteries, Nature 407 (2000) 496–499.

[30] T. Yang, Y.G. Liu, Z.H. Huang, Q. Yang, M. Guan, M.H. Fang, X. W. Wu, A facile strategy for fabricating hierarchically mesoporous Co_3O_4 urchins and bundles and their application in Li-ion batteries with high electrochemical performance, RSC Adv. 5 (2015) 24486–24493.

[31] B. Yan, L. Chen, Y.J. Liu, G.X. Zhu, C.G. Wang, H. Zhang, G. Yang, H. T. Ye, A.H. Yuan, Co_3O_4 nanostructures with a high rate performance as anode materials for lithium-ion batteries, prepared via book-like cobalt-organic frameworks, CrystEngComm 16 (2014) 10227–10234.

[32] J.H. Zhang, J. Du, Y.T. Qian, Q.H. Yin, D.J. Zhang, Shape-controlled synthesis and their magnetic properties of hexapod-like, flake-like and chain-like carbon-encapsulated Fe_3O_4 core/shell composites, Mater. Sci. Eng. B 170 (2010) 51–57.

[33] J.S. Chen, T. Zhu, Q.H. Hu, J.J. Gao, F.B. Su, S.Z. Qiao, X.W. Lou, Shape-controlled synthesis of cobalt-based nanocubes, nanodiscs, and nanoflowers and their comparative lithium-storage properties, ACS Appl. Mater. Interfaces 2 (2010) 3628–3635.

[34] J.H. Zhang, W. Sheng, B. Yan, L.B. Wang, Y.T. Qian, Graphene encapsulated Fe_3O_4 nanospindles as a superior anode material for lithium-ion batteries, J. Nanosci. Nanotechnol. 13 (2013) 4364–4369.

[35] N. Du, H. Zhang, B.D. Chen, J.B. Wu, X.Y. Ma, Z.H. Liu, Y.Q. Zhang, D.R. Yang, X.H. Huang, J.P. Tu, Porous Co_3O_4 nanotubes derived from $Co_4(CO)_{12}$clusters on carbon nanotube templates: a highly efficient material for Li-battery applications, Adv. Mater. 19 (2007) 4505–4509.

[36] J.Y. Wang, N.L. Yang, H.J. Tang, Z.H. Dong, Q. Jin, M. Yang, D. Kisailus, H.J. Zhao, Z.Y. Tang, D. Wang, Accurate control of multishelled Co_3O_4 hollow microspheres as high-performance anode materials in lithium-ion batteries, Angew. Chem. 125 (2013) 6545–6548.

[37] L. Zhang, H.B. Wu, X.W. Lou, Metal-organic-frameworks-derived general formation of hollow structures with high complexity, J. Am. Chem. Soc. 135 (2013) 10664–10672.

[38] C. Li, T.Q. Chen, W.J. Xu, X.B. Lou, L.K. Pan, Q. Chen, B.W. Hu, Mesoporous nanostructured Co_3O_4 derived from MOF template: a high-performance anode material for lithium-ion batteries, J. Mater. Chem. A 3 (2015) 5585–5591.

Please cite this article as: L. Zhang, et al., Design and self-assembly of metal-organic framework-derived porous Co_3O_4 hierarchical structures for lithium-ion batteries, Ceramics International (2015), http://dx.doi.org/10.1016/j.ceramint.2015.12.038